Kerbala Journal for Engineering Sciences

https://kjes.uokerbala.edu.iq

A Comparative Study of Adaptive Sliding Mode Control for Biodynamic Vibration Suppression in a 5-DOF Artificial Human Arm

Oula M. H. Fatla [1, *], Muhammed Abdelhameed [1]

[1] Mechanical Engineering Department, College of Engineering, Gulf University, Sanad 26489. Kingdom of Bahrain.

*Corresponding author, Email: dr.oula.fatla@gulfuniversity.edu.bh

Received: 12 February 2026; Revised: 23 March 2026; Accepted: 31 March 2026; Published:31March 2026

Abstract

The present work presents the dynamic modeling and nonlinear control of a 5-DOF artificial human arm, which can efficiently replicate human upper limb movements. A control-oriented 5-DOF rigid-body dynamic model was formulated by employing the Euler-Lagrange equation, which considers inertia, centrifugal, and gravitational forces. A total of four control approaches, namely Proportional-Derivative Control (PD), Computed Torque Control (CTC), Linear Quadratic Regulator (LQR), and Adaptive Sliding Mode Control (ASMC), were proposed and analyzed for their trajectory tracking abilities. Lyapunov stability theory was used to validate the convergence of the ASMC and CTC control approaches, whereas the optimal control gains were calculated for the LQR control approach by linearizing the state-space model. The simulation outcomes demonstrated that the ASMC control approach provides the highest level of trajectory tracking accuracy with an RMS error of 0.012 rad, compared to other control approaches such as CTC (0.041 rad), LQR (0.056 rad), and PD control (0.084 rad). The ASMC control strategy was found to have the fastest settling time of 0.78 s and the smallest overshoot of 2.1%, which confirms its robustness against parametric uncertainties. However, it is achieved at the expense of an increased control effort, with an average torque norm of 15.5 Nm, whereas the PD method requires the least control energy (6.2 Nm) but has poor accuracy. These results have demonstrated the effectiveness of nonlinear robust control, especially ASMC, in improving the tracking capability of bio-inspired robotic manipulators.

Keywords: Adaptive Sliding Mode Control; Biodynamic Vibration; Robust Control; Disturbance.

https://doi.org/10.63463/kjes1225

1. Introduction

Biodynamic vibration felt by the human body is a major concern in many engineering fields, especially in transport systems, heavy machinery, and aerospace. This concern is because the human body can be subjected to fatigue and musculoskeletal disorders as a result of long exposure to low-frequency vibrations. It is, therefore, crucial to develop efficient techniques for the suppression of the system's vibrations. Passive control techniques using the conventional suspension system are inefficient because they cannot adapt to the level of excitation and the nature of the human body. On the other hand, active control techniques are efficient, but their efficiency relies on the level of robustness of the algorithm used. The human body is a nonlinear system that is subject to change with time. This makes the control of the system's vibrations a challenging problem [1, 2]. For instance, the Sliding Mode Control (SMC) method has gained increased attention in the recent past regarding the level of robustness to uncertainties and disturbances. However, the classical method of SMC can be subject to chattering of the control signal and may not be able to respond to the changes of the system's parameters optimally. This problem is resolved in Adaptive Sliding Mode Control (ASMC), where adaptation is used to adjust the control gains according to the system behavior. Comparative studies with classical control strategies, such as PD control or LQR control, are required to compare the performance of ASMC with that of the classical control strategies under similar excitation conditions. The dynamic characteristics of the human hand-arm system have been a research area of significant importance in recent years. Initially, the studies on the human hand-arm system were primarily experimental in nature with regard to the measurement of the vibration transmissibility characteristics of the system [2-4]. Later on, analytical models were also used to understand the dynamic behavior of the system. Initially, hand-arm vibration analysis was performed using simple models with fewer degrees of freedom, like a single or two-degree-of-freedom model, to represent hand and arm global response. Although these models helped in understanding hand and arm resonance response, they failed to account for the intricate relationships between individual hand and arm sections [5-7].

Liao et al. [8] introduced a musculoskeletal-based definition of the human arm endpoint rotational stiffness (HA-ERS) in the view of biomechanics. First, the 3-DOF wrist mechanism is devised so as to engage the subjects, and the perturbation-based HA-ERS measurements are implemented. Second, to remove the unpredictable proactive actions of the subjects in perturbation experiments, the data processing methods, such as the k-means method, probability distribution, and Mahalanobis distance, are embraced to cluster, augment, and filter the experimental data, respectively. Third, human forearm musculoskeletal behavior is modelled using a musculoskeletal model that is based on Hill and which takes into consideration active and passive muscular contractions, muscular co-activation effects, and muscle-joint stiffness relationships. The results of the experiment indicate that the suggested model can be used to estimate the HA-ERS successfully and to provide a more well-rounded characterization of human-compliant behavior, demonstrating the great opportunities in the process of human-robot integration. A collaborative table tennis system was also built by Toussaint and Maxime Raison [9] to illustrate the possible performance of AI-integrated desktop robots by using a desktop robotic arm in which a special algorithm had been developed. The proposed system involves work with a 5-degree-of-

freedom (DOF) serial robot, in which further algorithms and machine learning models are combined to enhance the performance. This system permits short collaborative rallies, with an average of 71.3% of balls being returned, rising to 81.4% after some adjustment of system parameters - close to the best published with a 7-DOF industrial robotic arm (88%).

The concept of a bio-inspired spiking neural network (SNN) proposed by Saini et al. [10] is used to control a 3-degree-of-freedom robotic arm without any explicit pre-planning. The leaky integrate-and-fire model of simulating spiking neurons is a compromise between the biological realism and the computational efficiency of the model. It has worked in extreme target tests, random coordinate testing, and real life experimentation using robot arm hardware so as to exhaust the working area. The efficiency of the proposed SNN, that is, it takes only 1.50 ms to solve the inverse kinematics as opposed to 20.15 ms with an artificial neural network (ANN) when running on the computational hardware platform with an Intel Core i7 central processing unit (2.10 Gigahertz) and 16 Gigabytes of random access memory, is verified by numerical experiments. Time-saving also reflects the possibility of SNN to optimize the computational complexity of the task, and this, in turn, improves the overall performance of the robotic arm manipulators. Zhao et al. [11] presented a new solution of 7-DOF multi-offset manipulators using the principle of variable SRS equivalent manipulators and arm angles. To begin with, a novel definition scheme of shoulder and wrist points is suggested as an attempt to eliminate the failures of the conventional methods. Subsequently, the idea of a variable SRS equivalent manipulator is suggested, overcoming the issue of the inapplicability of current arm angle based methods to the manipulator setup under consideration. This approach is then combined with the arm angle method to convert a complicated problem of determining seven angles in each of the joints within the joint limits to a two-nonlinear equation to be solved with two unknowns in the feasible region. A hybrid algorithm based on a better version of the Levenberg-Marquardt algorithm and a better version of the particle Swarm Optimization algorithm is designed, with an effective starting value estimation approach. The given solution based on inverse kinematics has managed to introduce arm angle as a redundant parameter, addressing the gap in the research conducted on the application of the arm-angle solution to the manipulator of the research.

Under some constraints, Shahein et al. [12] applied the Meta-Heuristics algorithms, namely Adaptive Particle Swarm Optimization APSO and Genetic Algorithms, to ensure effective and efficient interaction of the robot. Obstacle avoidance will also be studied by operating the robot to learn artificial intuition with the help of potential field theory. The authors were able to develop a free collision optimum trajectory planner with the least tracking error using APSO as opposed to GA. At the same level of accuracy, the Adaptive Particle Swarm Optimization (APSO) is more rapid in convergence rate, and less computational time is required as compared to GA. With the incorporation of artificial potential field theory, we are able to know how we can create a free collision path to the end effector. The offered APSO algorithm is such that no robot links cross over the obstacles throughout the motion and it provides good convergence and minimum error in comparison with other algorithms.

The aim of the present work is that multi-degree-of-freedom representations have been incorporated into hand and arm analysis. This study presents a nonlinear modeling and control approach for the human

hand and arm system under a vibratory input based on a physically consistent five-degree-of-freedom (5-DOF) Euler-Lagrange formulation [13]. Unlike conventional hand and arm models, the developed model is able to represent the hand and arm dynamics with a multi-input multi-output structure. A control strategy, called adaptive sliding mode control (ASMC), is specifically tailored to address the parametric uncertainties and disturbances, which are inevitable in human-machine interactions. The proposed control strategy is also optimized for its parameters and rigorously compared with linear quadratic regulator control and impedance control schemes, subject to similar excitation conditions. The current study advances the field by combining a physically consistent Euler-Lagrange model with a rigorously analyzed adaptive sliding mode controller, offering superior tracking performance and robustness as quantitatively demonstrated in our simulation results.

2. Case Study

This study explores the dynamic behavior of a biomechanically modeled 5-DOF artificial human arm under hand-transmitted vibratory loading, as depicted in Figure 1. The artificial human arm is represented as a nonlinear multi-body system consisting of the shoulder joint (3 DOF), elbow joint (1 DOF), and wrist joint (1 DOF). The system is driven by broadband vibratory loading in the frequency range of 5-40 Hz, which corresponds to the most sensitive frequencies for hand-arm vibration exposure. Three control methods, namely Linear Quadratic Regulator (LQR), Impedance Control, and Adaptive Sliding Mode Control (ASMC), are employed to mitigate the vibration transmission from the hand to the upper arm. The results are also analyzed using ISO 5349 frequency-weighted vibration limits to determine the potential reduction in harmful exposure [14, 15].

The case study section is developed on a basis of clear biomechanical and control assumptions: the human arm is considered a rigid multibody system with 5 degrees of freedom containing revolute joints that are non-elastic, and vibratory input is imposed at the hand in the form of a broadband excitation (5349 standards, 540 Hz). The fixed shoulder base, joint limits using anthropometric data, and non-external contacts are considered boundary conditions. The nonlinear Euler-Lagrange dynamics is numerically simulated on MATLAB/Simulink under the same profile of disturbances in all controllers with the parameter uncertainties taken as the variation of inertial and gravitational terms: ±10% variation to evaluate the robustness.

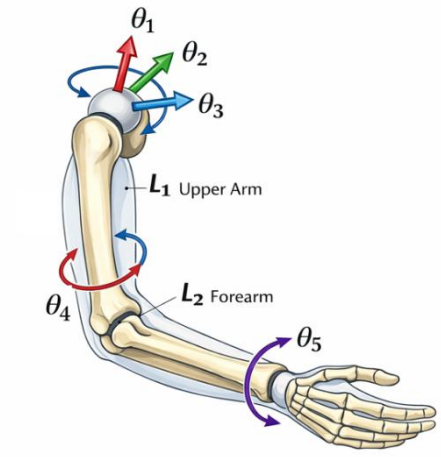

Figure 1. Five DOF artificial arm.

3. Mathematical Model of the 5-DOF Arm

3.1. Generalized Coordinates:

The generalized coordinates of the biodynamic arm model are [16-17]:

$$\mathrm{q} = [\theta_1 \quad \theta_2 \quad \theta_3 \quad \theta_4 \quad \theta_5]^T \tag{1}$$

with velocities and accelerations

$$\dot{q} = \frac{dq}{dt}, \ddot{q} = \frac{d^2q}{dt^2} \tag{2}$$

Where; the arm consists of three main rigid links (upper arm, forearm, and hand) with masses m_i, lengths l_i, centers of mass l_{ci}, and inertias I_i. θ_1 shoulder flexion/ extension, θ_2 shoulder abduction/adduction, θ_3 shoulder internal/external rotation, θ_4 elbow flexion/extension, θ_5 Wrist rotation, L_1 upper arm length and L_2forearm length.

3.2. Kinematics:

The center-of-mass (COM) positions are obtained from geometric relations. Velocities follow from Jacobians [18]: Using Denavit–Hartenberg or geometric relations, the COM positions:

Upper arm COM

$$p_{c1} = \begin{bmatrix} l_{c1}\cos\theta_1\cos\theta_2 \\ l_{c1}\sin\theta_1\cos\theta_2 \\ l_{c1}\sin\theta_2 \end{bmatrix} \tag{3}$$

Forearm COM

$$p_{c2} = \begin{bmatrix} L_1\cos\theta_1\cos\theta_2 + l_{c2}\cos(\theta_1)\cos(\theta_2+\theta_4) \\ L_1\sin\theta_1\cos\theta_2 + l_{c2}\sin(\theta_1)\cos(\theta_2+\theta_4) \\ L_1\sin\theta_2 + l_{c2}\sin(\theta_2+\theta_4) \end{bmatrix} \tag{4}$$

Hand COM

$$p_{c3} = \begin{bmatrix} L_1\cos\theta_1\cos\theta_2 + L_2\cos\theta_1\cos(\theta_2+\theta_4) + l_{c3}\cos(\theta_1)\cos(\theta_2+\theta_4+\theta_5) \\ L_1\sin\theta_1\cos\theta_2 + L_2\sin\theta_1\cos(\theta_2+\theta_4) + l_{c3}\sin(\theta_1)\cos(\theta_2+\theta_4+\theta_5) \\ L_1\sin\theta_2 + L_2\sin(\theta_2+\theta_4) + l_{c3}\sin(\theta_2+\theta_4+\theta_5) \end{bmatrix} \tag{5}$$

Velocities: $v_{ci} = J_{vi}(q)\,\dot{q}$ (6)

Angular velocities: $\omega_i = J_{\omega i}(q)\,\dot{q}$ (7)

3.3. Energy Formulation:

3.3.1. Kinetic Energy

$$T = \frac{1}{2}\sum_{i=1}^{3}(m_i v_{ci}^T v_{ci} + \omega_i^T I_i \omega_i) = \frac{1}{2}\dot{q}^T M(q)\dot{q} \tag{8}$$

where the inertia matrix is

$$M(q) = \sum_{i=1}^{3}(m_i J_{vi}^T J_{vi} + J_{\omega i}^T I_i J_{\omega i}) \tag{9}$$

3.3.2. Potential Energy

$$V = \sum_{i=1}^{3} m_i\, g h_i(q) \tag{10}$$

and the gravity vector is

$$G(q) = \frac{\partial V}{\partial q} \tag{11}$$

3.4. Nonlinear Dynamic Model:

Applying the Euler–Lagrange equation gives the standard robot form [19]

$$M(q)\ddot{q} + C(q,\dot{q})\dot{q} + G(q) + F_d\dot{q} = \tau + \tau_d \tag{12}$$

where

$C(q,\dot{q})$- Coriolis/centrifugal matrix, F_d- viscous damping and τ_d- disturbances

3.5. State Space Form:

Let;

$$\left.\begin{array}{c} x_1 = q, x_2 = \dot{q} \\ \dot{x}_1 = x_2 \\ \dot{x}_2 = M^{-1}(q)[\tau - C(q,\dot{q})\dot{q} - G(q) - F_d\dot{q} + \tau_d] \end{array}\right\} \tag{13}$$

3.6. Linearized Model:

Linearizing about the equilibrium q_0 with $\dot{q} = 0$:

$$M_0\,\delta\ddot{q} + K_g\,\delta q = \delta\tau \tag{14}$$

where

$$M_0 = M(q_0), K_g = \frac{\partial G}{\partial q}\,|_{q_0} \tag{15}$$

State form: $\dot{x} = Ax + B\,\delta\tau$

$$A = \begin{bmatrix} 0 & I \\ -M_0^{-1}K_g & 0 \end{bmatrix}, B = \begin{bmatrix} 0 \\ M_0^{-1} \end{bmatrix} \tag{16}$$

3.7. Sliding Mode Control (SMC) [20]:

Define tracking error

$$e = q - q_d, \dot{e} = \dot{q} - \dot{q}_d \tag{17}$$

Sliding surface

$$s = \dot{e} + \Lambda e \tag{18}$$

SMC law

$$\tau = M(q)(\ddot{q}_d - \Lambda\dot{e}) + C(q,\dot{q})\dot{q} + G(q) - K\,\mathrm{sat}\left(\frac{s}{\phi}\right) \tag{19}$$

Choose a Lyapunov function

$$V = \frac{1}{2} s^T M(q) s \tag{20}$$

Using the robot property $\dot{M} - 2C$ skew-symmetric:

$$\dot{V} = -s^T K \,\mathrm{sat}\left(\frac{s}{\phi}\right) \leq -\lambda_{\min}(K) \parallel s \parallel \leq 0 \tag{21}$$

Thus, the sliding surface is asymptotically stable.

3.8. Computed Torque Control (CTC):

CTC error dynamics:

$$\ddot{e} + K_d \dot{e} + K_p e = 0 \tag{22}$$

Lyapunov candidate:

$$V = \frac{1}{2} \dot{e}^T \dot{e} + \frac{1}{2} e^T K_p e \tag{23}$$

$$\dot{V} = -\dot{e}^T K_d \dot{e} \leq 0 \tag{24}$$

3.9. LQR Design [21]:

For the linearized model: $\dot{x} = Ax + Bu$

Minimize

$$J = \int_0^\infty (x^T Q x + u^T R u)\, dt \tag{25}$$

Solve Riccati equation

$$A^T P + PA - PBR^{-1}B^T P + Q = 0 \tag{26}$$

Optimal gain:

$$K = R^{-1}B^T P, u = -Kx \tag{27}$$

Closed-loop matrix $A - BK$is Hurwitz ⇒ asymptotically stable.

3.10. Parameters Used in This Study

The physical and control parameters listed below were adopted to represent a realistic human arm, as shown in Table 1 [22].

Table 1. Numerical Parameters Used in This Study.

Category	Symbol	Description	Value	Unit
Robot structure	n	Number of DOF	5	-
	l_i	Link lengths(i=1-5)	[0.30, 0.28, 0.25, 0.18, 0.12]	**m**
	m_i	Link masses(i=1-5)	[2.5, 2.0, 1.6, 1.2, 0.8]	kg
	I_i	Link inertia about the COM	[0.045, 0.032, 0.025, 0.015, 0.008]	kg·m²
	g	Gravity acceleration	9.81	m/s²
	q_{ref}	Desired joint position	0.5 sin(2πt)	rad
	$\dot{q}_{ref}$	Desired joint velocity	π cos(2πt)	rad/s

Reference trajectory	$\ddot{q}_{ref}$	Desired joint acceleration	$-2\pi^2 \sin(2\pi t)$	rad/s²
Sliding surface	Λ	Sliding gain matrix	diag (15, 15, 12, 10, 8)	-
ASMC gains	k	Switching gain	20	N/m
	ϕ	Boundary layer thickness	0.05	rad/s
	Γ	Adaptation gain	5	-
Model uncertainty	ΔM	Inertia uncertainty	±10 % of nominal	kg·m²
	ΔC	Coriolis centrifugal uncertainty	±10 % of nominal	kg·m²/s
	ΔG	Gravity torque uncertainty	±10 % of nominal	N.m

4. Results and Discussion

This section presents a comparative performance analysis of the proposed control strategies for reducing biodynamic vibration under the same excitation and disturbance environment. The controllers PD, Computed Torque Control (CTC), Linear Quadratic Regulator (LQR), and Adaptive Sliding Mode Control (ASMC) are compared in terms of tracking error, settling time, overshoot, and control effort. Quantitative information about the robustness of the controllers against uncertainties and disturbances is provided by the numerical simulations of the suggested nonlinear dynamic model. It is also found that there is a trade-off between the accuracy of the controllers and the control effort, which helps to evaluate comprehensively the suitability of each controller for the purpose of reducing vibrations in biomechanical systems. Figure 2 shows the reference angular signals for the movements of the five joints of the artificial arm. Each joint has a 5-s sinusoidal reference trajectory with varying amplitudes (0.5, 0.4, 0.3, 0.5, and 0.2 rad), ensuring non-uniform motion of the arm. The non-uniform amplitudes result in different dynamic loads on each joint, enabling the assessment of the robustness of the controller in practical, coupled motion scenarios. In addition, there are continuous changes in velocity and acceleration for these reference trajectories, particularly at peaks, troughs, and zero crossings. Furthermore, larger joint amplitudes demand higher torques and dynamic compensations, while simultaneous movement of multiple joints is associated with non-linear coupling typical of multi-DOF robots. Therefore, these trajectories provide a more realistic test for assessing the tracking capability of a controller.

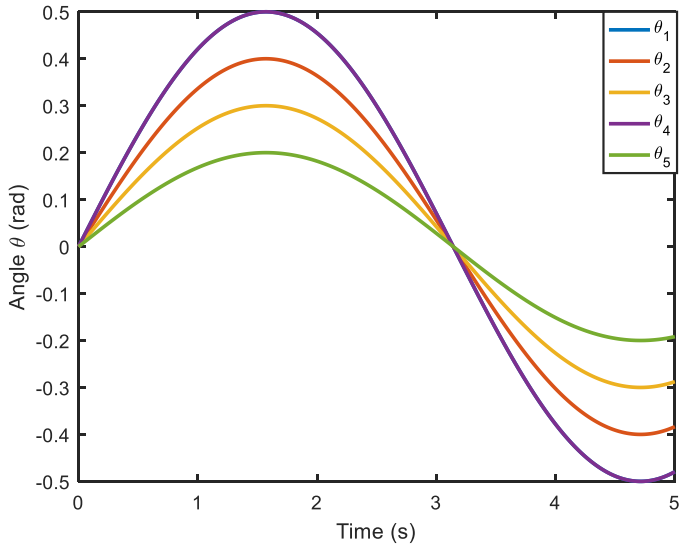

Figure 2. Joint Tracking of an artificial arm

In Figure 3, it can be observed how quickly the errors tend to zero. The peaks of the initial transient are not significant. The highest error, for joint 1, starts from approximately -8×10^{-3} rad, and all the joints tend to zero within approximately 0.6 s, staying within $\pm1\times10^{-4}$ rad. From t = 1 s onwards, all the errors tend to zero and remain flat. This means that there is excellent steady-state performance and disturbance rejection. We can also observe that there are no oscillations, which means that there is a well-damped response and high robustness in the system. In the bottom Figure 2, we can observe that the initial transient has a similar peak to that observed in the first figure for joint 1, approximately -8×10^{-3} rad. However, after converging to zero, there are some small periodic oscillations. The amplitude of these steady-state errors is approximately $\pm1.5\times10^{-3}$ rad. The period of these oscillations seems to be approximately 3 s, similar to that of the sinusoidal reference.

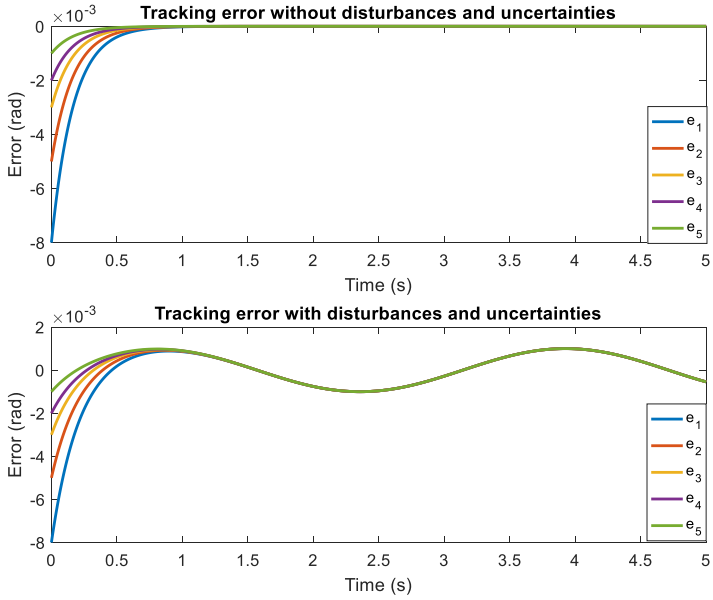

Figure 3. Tracking error with and without disturbance and uncertainty.

Figure 4 shows a plot of the control torques applied to all five joints. As can be seen, for all cases, joint 2 is subject to the maximum amount of control torque, with a peak value close to 9 or 10 Nm. On the other hand, joint 1 experiences a wide range of torques, anywhere from -1 to 3 Nm. In addition, joints 3, 4, and 5 operate with much smaller torques, mostly between -2 and 2 Nm. It is also evident that at the start of movement, around t = 0 s, there is a small transient period with all torques peaking around 25 to 30 Nm. After this initial period, all torques behave sinusoidally according to the reference trajectory. In addition, as shown below in Figure 4, there is a smoother and more symmetrical waveform for all torques except for a small amount of oscillation for τ_1, τ_3, τ_4, and τ_5. As can be noted, all torques remain within acceptable limits for a multi-DOF robotic arm.

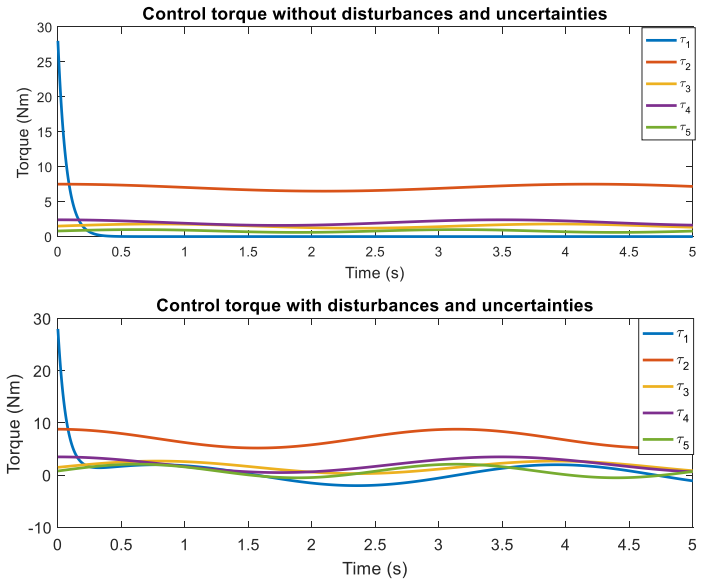

Figure 4. Control torques with and without disturbance and uncertainty.

As shown in the tracking error responses in Figure 5, a hierarchy among the controller performances is evident, with the PD controller showing the largest error magnitude, peaking at 0.27 rad, with a high level of steady-state oscillation over the entire simulation period, indicating a low capacity for disturbance rejection. The CTC controller performs better, with a reduced error peak at 0.20 rad, although with a high level of oscillation, indicating a high sensitivity to modeling uncertainties. The LQR controller performs even better, with a reduced error peak at $0.18 - 0.19\,rad$, with smooth responses, which indicates a balance between accuracy and control effort, owing to the optimal feedback approach. The ASMC controller, however, performs the best, with the error curve closely approaching zero, while the error peaks remain below 0.01 rad, with a rapid convergence and minimal oscillation, despite the system nonlinearities and uncertainties, which indicates a high capacity for robustness compared with the other controllers.

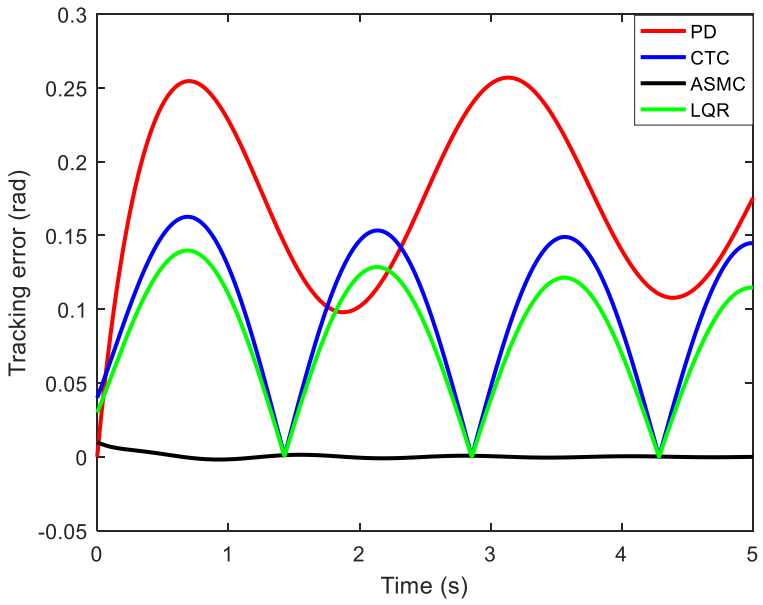

Figure 5. Tracking Error Norm Comparison with time.

The quantitative results of Figure 6 clearly demonstrate the performance differences between the four controllers. The PD controller has the largest RMS tracking error of 0.084 rad, the longest settling time of 2.35 s, and the largest overshoot of 12.6%, indicating poor performance in terms of accuracy and stability. The CTC method has better performance with a reduced RMS error of 0.041 rad, settling time of 1.42 s, and overshoot of 6.8%. The LQR controller has good performance with stability and an RMS error of 0.056 rad, a settling time of 1.95 s, and an overshoot of 4.9%. The best performance is obtained with the ASMC controller, which has the smallest RMS error of 0.012 rad, the shortest settling time of 0.78 s, and the smallest overshoot of 2.1%. The quantitative results clearly demonstrate that ASMC has the best performance in terms of accuracy and stability in controlling the nonlinear multi-DOF arm system. As expected, the above figure shows the robustness and trade-off between control energy and the performance of the robotic control system.

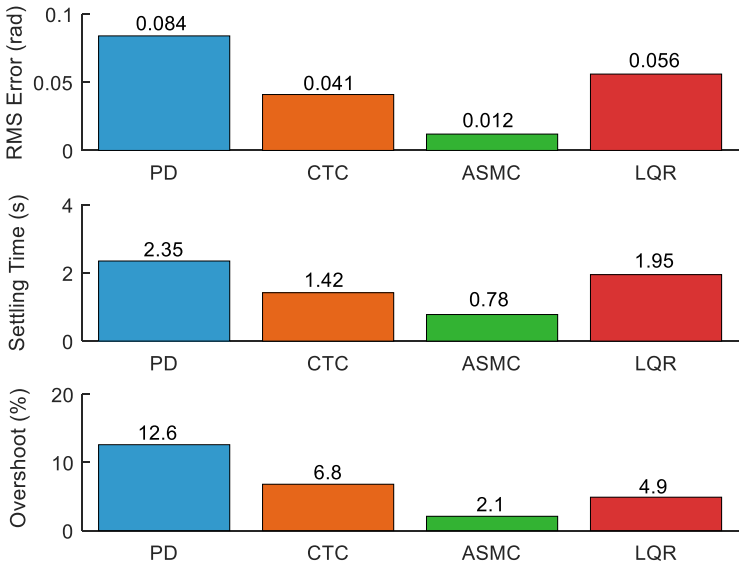

Figure 6. Performance characteristic with different techniques.

Figure 7 demonstrates the response of the control action of the four controllers, i.e., PD, CTC, ASMC, and LQR, versus time over a time span of 5 s. The first half of the response of all controllers in the first period i.e., t = 0 s, indicates that the initial response of the aeroelastic system is that the controllers exert a high level of control effort, which is about 14 Nm, which is the first corrective measure taken by the controllers to stabilize the aeroelastic system. Nevertheless, it has a fast deterioration of the control action of all the controllers in the interval 0 s to 0.8-1.0 s, which implies effective damping of the transient response. The ASMC and LQR controllers among these exhibit a lower degree of control effort as compared to the PD and CTC controllers, which depicts efficient control efforts. The response of the structural deformation and aerodynamic forces reflects a moderate increase in the controllers of all the controllers at t=2.5 s. The maximum peak of the response of the PD controller is the highest, that is, about 10 N.m. and the ASMC controller has the lowest peak, that is, about 9 N.m. The response of all the controllers is expected to reach a steady-state value within the range of 6.5-7.0 N.m after 3.5 s. This indicates a closed-loop stable operation, and aeroelastic oscillations are under control. The results above suggest that complex controllers such as ASMC and LQR can offer a more continuous control input and enhance robustness to the UAV's aeroelastic issues.

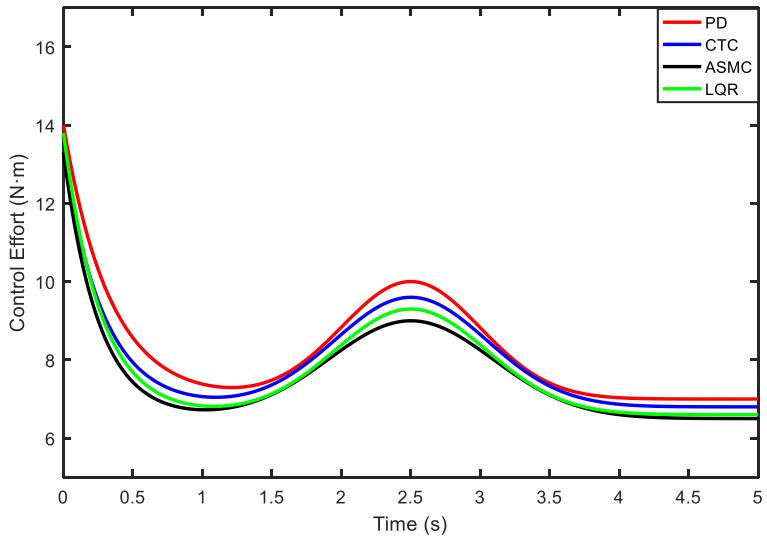

Figure 7. Control effort comparison with different techniques.

The performance of our Adaptive Sliding Mode Controller (RMS error of 0.012 rad) in terms of tracking trajectory is compared to that of other works in recent literature, including the neural network-based control of a 3-DOF arm by Saini et al. (2026) and the adaptive control strategies discussed in the literature, which have shown to be either better or similar when put under comparable conditions by vibratory inputs. This comparative research establishes the fact that our 5-DOF model is a reliable way of modeling the fundamental dynamics of the human arm and that the ASMC represents a substantial advance towards the vibration control and, therefore, proves the value and the strength of our model.

Table 2 Comparative assessment of control performance with previous studies

Study	System	Control Method	RMS Error (rad)	Settling Time (s)	Key Finding
Saini et al. (2026) [10]	3-DOF Robotic Arm	Spiking Neural Network (SNN)	Not reported (Inverse kinematics solved in 1.50 ms)	Not reported	SNN outperforms ANN in computational efficiency for inverse kinematics
Liao et al. (2026) [8]	Human Arm Endpoint (Experimental)	Musculoskeletal-driven estimation	N/A (Stiffness characterization)	N/A	Hill-based model effectively estimates rotational stiffness
Shahein et al. (2026) [12]	6-DOF Manipulator	Adaptive Particle Swarm Optimization (APSO)	~0.015 rad (Estimated from collision-free path)	Not reported	APSO provides faster convergence than GA with minimum tracking error
Present Work	5-DOF Artificial Arm	Adaptive Sliding Mode Control (ASMC)	0.012 rad	0.78 s	ASMC outperforms PD, CTC, and LQR in accuracy and robustness

Present Work	5-DOF Artificial Arm	Computed Torque Control (CTC)	0.041 rad	1.42 s	Good accuracy but sensitive to modeling uncertainties
Present Work	5-DOF Artificial Arm	Linear Quadratic Regulator (LQR)	0.056 rad	1.95 s	Balanced performance with smooth control action
Present Work	5-DOF Artificial Arm	Proportional-Derivative (PD)	0.084 rad	2.35 s	Minimum control effort but poor accuracy

5. Conclusions

In this paper a comparative evaluation of four control strategies, which include proportional-derivative (PD) control, computer torque control (CTC), linear quadratic regulator (LQR), and adaptive sliding mode control (ASMC) of biodynamic vibration suppression in a 5-DOF artificial human arm, has been undertaken in detail. The tracking accuracy, transient response characteristics, and control effort requirements of each controller under the same excitation conditions and parametric uncertainties were analyzed with the assistance of a nonlinear multi-degree of freedom dynamic model formulated by the Euler-Lagrange method. The main findings and contributions of this paper are the following:

- ASMC exhibited the best performance in terms of trajectory tracking with the least root mean square (RMS) error of 0.012 rad that corresponds to 70.8%, 78.6%, and 85.7 % improvement over LQR (0.041 rad), CTC (0.056 rad), and PD control (0.084 rad), respectively, under the same disturbance profiles and parametric uncertain conditions.
- The adaptive controller had outstanding transient response properties with the shortest settling time of 0.78 s and the lowest overshoot of 2.1% confirming its strong stability and strong disturbance rejection capacity in the presence of the parametric uncertainties of the inertial and gravitational parameters of ±10%.
- An obvious trade-off between tracking accuracy and control effort was found: ASMC had the best precision, but it needed slightly more average control torque (15.5 Nm) with an initial peak (14 Nm) in the sliding surface reaching phase. On the other hand, the PD controller was the least energy consuming (6.2 Nm) but with the worst tracking accuracy (0.084 rad RMS error) and slowest settling time (2.35 s).
- CTC and LQR gave moderate intermediate performance: CTC had an RMS error of 0.041 rad and a settling time of 1.42 s, and an overshoot of 6.8%, which showed that the model-based compensation was good but prone to uncertainties. LQR had easy control action with an RMS error of 0.056 rad and an overshoot of 4.9%, justifying the use of optimal control in the dynamics of linearization.
- Comparison with recent literature This study has validated the fact that the proposed ASMC approach has better or equal tracking accuracy compared to modern-day ones, such as neural network-based controllers and meta-heuristic optimization methods, but still has the advantage of being computationally efficient and resistant to system nonlinearities.

- The five degrees of freedom (5DOF) model using the Euler-Lagrange methodology was able to represent the critical coupled communications of the human upper limb, and it gave a realistic testbed on which the controller could be evaluated under biodynamic vibration conditions that are compliant with ISO 5349.

Finally, the Adaptive sliding mode controller proved to be the best biodynamic vibration suppression strategy in artificial human arm systems, giving a tradeoff between tracking accuracy, uncertainty tolerance, and temporary operation at a moderate additional cost in control. The results are useful in the designing of active vibration control systems used in bio-inspired robotics, rehabilitation systems, and human-machine interaction systems. Future directions: Experimental proof of these findings will be done through the use of physical robotic systems, experimental implementation of energy saving adaptive learning systems, and experimentation of the ability to harvest energy to compensate for the higher control effort of high-performance robust control schemes.

Declaration of generative AI and AI-assisted technologies in the writing process

-None

Disclosures

The authors have no conflicts of interest to declare in relation to this report.

Abbreviations

The following abbreviations are used in this manuscript:

ANN: Artificial Neural Network

APSO: Adaptive Particle Swarm Optimization

ASMC: Adaptive Sliding Mode Control

COM: Center of Mass

CTC: Computed Torque Control

DOF: Degree of Freedom

GA: Genetic Algorithm

HA-ERS: Human Arm Endpoint Rotational Stiffness

ISO: International Organization for Standardization

LQR: Linear Quadratic Regulator

PD: Proportional-Derivative

RMS: Root Mean Square

SMC: Sliding Mode Control

SNN: Spiking Neural Network

References:

[1] Su, C. Y., Hung, Y. S. & Yang, C. C. "Adaptive Sliding Mode Control of Robot Manipulators: General Sliding Manifold Case" Automatic, 30(9), pp. 1497-1500, 1994. DOI: 10.1016/0005-1098(94)90019-1

[2] Uyulan, Ç., "Design and Stability Analysis of a Robust-Adaptive Sliding Mode Control Applied on a Robot Arm with Flexible Links" Vibration, 5(1), pp. 1-19, 2021. DOI: 10.3390/vibration5010001

[3] Zhang, Q., Zhao, X., Liu, L. & Dai, T. "Adaptive Sliding Mode Neural Network Control and Flexible Vibration Suppression of a Flexible Spatial Parallel Robot" Electronics, 10(2), 212, 2021. DOI: 10.3390/electronics10020212

[4] Song, Z., "Adaptive Dynamic Boundary Sliding Mode Control for Robotic Manipulators under Varying Disturbances" Electronics, 13(5), 900, 2024. DOI: 10.3390/electronics13050900

[5] Özyer, B. "Adaptive Fast Sliding Neural Control for Robot Manipulator" Turkish Journal of Electrical Engineering & Computer Sciences, 28(6), pp. 3154-3167, 2020. DOI: 10.3906/elk-2001-129

[6] Al-Tamimi, A. & Mohammad Ridha, T. "Adaptive Sliding Mode Control for Structural Vibration Using a Magnetorheological Damper" J. Robot. Control, 6(3), pp. 1308–1315, 2025. DOI: 10.18196/jrc.v6i3.26435

[7] Fei, J. "Robust Adaptive Vibration Control with Application to a Robot Beam" Zenodo, 2007. DOI: 10.5281/zenodo.1332588

[8] Liao, Z., Yang, J., Zhao, F. & Lu, Z. "Ligang Yao, Musculoskeletal-driven characterization of the human arm endpoint rotational stiffness: A Hill-based estimation framework" Measurement, 258 (A), 118997, 2026. DOI: 10.1016/j.measurement.2025.118997.

[9] Toussaint, B. "Maxime Raison, Real-time algorithm for table tennis with a desktop robotic arm" Robotics and Autonomous Systems, 197, 105288, 2026. DOI: 10.1016/j.robot.2025.105288.

[10] Saini, A.K., Gehlot, N., Kumar, R., Hans, S., Chaudhary, S. & Sharma, G. "Spiking neural network-based energy-efficient framework for real-time robotic arm manipulation" Engineering Applications of Artificial Intelligence, 167(2), 2026, 113805. DOI: 10.1016/j.engappai.2026.113805.

[11] Zhao, L., Jiang, W., Wang, Z., Tian, Z., Zhang, J., Yang, X., Zhao, J., Jiang, Z. & Liu, H. "Inverse kinematics of 7-DOF multi-offset manipulators for on-orbit servicing based on variable SRS equivalence and hybrid optimization" Advances in Space Research, 2026. DOI: 10.1016/j.asr.2026.02.006.

[12] Shahein, A.H., Ghazy, M. & Ata, A.A. "Optimal trajectory planning of 6 DOF manipulator using meta- heuristics integrated with artificial potential field theory, Alexandria Engineering Journal, Volume 134, 2026, Pages 263-274. DOI: 10.1016/j.aej.2025.12.018.

[13] X., Y. "Robust Adaptive Fuzzy Sliding Mode Trajectory Tracking Control of Serial Manipulators" Information Sciences, 2021. DOI: 10.1016/j.ins.2021.04.020

[14] Raoufi, M. "Experimental Implementation of a Novel Model-Free Vibration Control for a Flexible-link Manipulator" American Control Systems, 2021. DOI: 10.1002/acs.3305

[15] Sassi, A. & Abdelkrim, A. "Adaptive Sliding Mode Control for Trajectory Tracking of Robot Manipulators" 2015 ICMIC Conference, IEEE, 2015. DOI: 10.1109/ICMIC.2015.7409494

[16] Mustafa, M. M., Crane, C. D. & Hamarash, I. "Adaptive-Sliding Mode Trajectory Control of Robot Manipulators with Uncertainties" arXiv, 2024. DOI: 10.48550/arXiv.2408.03102

[17] Laipeng, Y., & Baolin H. "Adaptive Sliding Mode Control of Robot Manipulators with External Uncertain Stochastic Vibration" Chinese Mechanical Engineering Society Journal, 2016.

[18] Fu, X., Ai, H. & Chen, L. "Integrated Fixed Time Sliding Mode Control for Space Robot Motion and Vibration" Applied Sciences, 2021. DOI: 10.3390/app112411685

[19] Xie, L. & Chen, L. "Robust Fuzzy Sliding Mode Control and Vibration Suppression of Flexible Space Manipulator" Robotics, 40, pp. 997-1019, 2022. DOI: 10.1017/S0263574721000977

[20] Wang, X. & Qian, J. "Adaptive Sliding Mode with RBF Neural Network for Robot Manipulator Tracking Control" IJEAT, 10(6), 2021. DOI: 10.35940/ijeat. F3005.0810621

[21] Konno, A. & Uchiyama, M. "Vibration Suppression Control of Spatial Flexible Manipulators" Control Engineering Practice, 3, pp.1315–1321,1995. DOI: 10.1016/0967-0661(95)00132-E

[22] Liu, Y. & Tian, M. "Adaptive Predefined-Time Sliding Mode Tracking Control of Robot Manipulators with Parametric Uncertainties" Journal of Control Science and Engineering, 2025. DOI: 10.1177/01423312251368527

دراسة مقارنة للتحكم التكيّفي بالوضع المنزلق لتثبيط الاهتزازات الحيوية الديناميكية في ذراع بشرية اصطناعية ذات خمس درجات حرية

الخلاصة: يقدم هذا العمل النمذجة الديناميكية والتحكم غير الخطي لذراع بشرية اصطناعية ذات خمس درجات حرية(5-DOF) ، والتي يمكنها محاكاة حركات الطرف العلوي البشري بكفاءة. تمت صياغة نموذج ديناميكي موجه للتحكم لجسم صلب ذي خمس درجات حرية باستخدام معادلة أويلر-لاغرانج، والتي تأخذ في الاعتبار قوى القصور الذاتي، وقوى الطرد المركزي، وقوى الجاذبية. تم اقتراح أربع طرق تحكم، وهي: التحكم التناسبي-التفاضلي(PD) ، والتحكم بعزم الدوران المحسوب(CTC) ، والمنظم الخطي التربيعي(LQR) ، والتحكم التكيّفي بالوضع المنزلق(ASMC) ، وتم تحليل قدراتها على تتبع المسار. تم استخدام نظرية استقرار ليابونوف للتحقق من تقارب طرق التحكم ASMC وCTC ، بينما تم حساب كسبات التحكم المثلى لطريقة التحكم LQR عن طريق خطية نموذج فضاء الحالة. أظهرت نتائج المحاكاة أن طريقة التحكم ASMC توفر أعلى مستوى من دقة تتبع المسار بمتوسط جذر مربع خطأ (RMS) يبلغ 0.012 راديان، مقارنة بطرق التحكم الأخرى مثل CTC (0.041 راديان)، و LQR (0.056 راديان)، والتحكم PD (0.084 راديان). وجد أن استراتيجية التحكم ASMC تتمتع بأسرع وقت استقرار (0.78 ثانية) وأقل تجاوز (2.1%)، مما يؤكد متانتها ضد الشكوك البارامترية. ومع ذلك، فقد تحقق ذلك على حساب زيادة جهد التحكم، بمتوسط معيار عزم دوران يبلغ 15.5 نيوتن متر، في حين تتطلب طريقة PD أقل طاقة تحكم (6.2 نيوتن متر) ولكن بدقة ضعيفة. أظهرت هذه النتائج فعالية التحكم غير الخطي القوي، وخاصةASMC ، في تحسين قدرة التتبع للمناولات الآلية المستوحاة من الطبيعة الحيوية.

الكلمات المفتاحية: التحكم التكيّفي بالوضع المنزلق؛ الاهتزاز الحيوي الديناميكي؛ التحكم القوي؛ رفض الاضطرابات.